The Astrophysical Journal, 893:7 (11pp), 2020 April 10 https://doi.org/10.3847/1538-4357/ab7cd1

Quasi-periodic Pulsation Detected in Lyα Emission During Solar Flares

Dong Li[1,2,3], Lei Lu[1], Zongjun Ning[1], Li Feng[1], Weiqun Gan[1], and Hui Li[1]
[1] Key Laboratory of Dark Matter and Space Astronomy, Purple Mountain Observatory, CAS, Nanjing 210033, People's Republic of China; lidong@pmo.ac.cn, leilu@pmo.ac.cn
[2] State Key Laboratory of Space Weather, Chinese Academy of Sciences, Beijing 100190, People's Republic of China
[3] CAS Key Laboratory of Solar Activity, National Astronomical Observatories, Beijing 100101, People's Republic of China
Received 2020 January 19; revised 2020 March 1; accepted 2020 March 3; published 2020 April 8

Abstract

We investigated the quasi-periodic pulsation (QPP) in Lyα, X-ray, and extreme-ultraviolet (EUV) emissions during two solar flares, i.e., an X-class (SOL2012-01-27T) and a C-class (SOL2016-02-08T). The full-disk Lyα and X-ray flux during these solar flares were recorded by the EUV Sensor and X-Ray Sensor on board the Geostationary Operational Environmental Satellite. The flare regions were located from the EUV images measured by the Atmospheric Imaging Assembly. The QPP could be identified as a series of regular and periodic peaks in the light curves, and its quasi-periodicity was determined from the global wavelet and Fourier power spectra. A quasi-periodicity at about 3 minutes is detected during the impulsive phase of the X-class flare, which could be explained as the acoustic wave in the chromosphere. Interestingly, a quasi-periodicity at roughly 1 minute is discovered during the entire evolutionary phases of solar flares, including the precursor, impulsive, and gradual phases. This is the first report of 1 minute QPP in the Lyα emission during solar flares, in particular during the flare precursor. It may be interpreted as a self-oscillatory regime of the magnetic reconnection, such as magnetic dripping.

Unified Astronomy Thesaurus concepts: Solar flares (1496); Solar oscillations (1515); Solar chromosphere (1479); Solar ultraviolet emission (1533); Solar x-ray emission (1536)

1. Introduction

Quasi-periodic pulsation (QPP) is a frequently observed feature during flare emissions on the Sun or Sun-like stars. A typical QPP is often regarded as the temporal and regular fluctuation of electromagnetic radiation in solar/stellar flares (see, i.e., Nakariakov & Melnikov 2009; Van Doorsselaere et al. 2016; McLaughlin et al. 2018, for reviews), which conveys the temporal feature and plasma characteristics of the flare radiation. Therefore, it should be useful to diagnose the coronal parameters of the Sun or remote Sun-like stars (e.g., Pugh et al. 2019; Yuan et al. 2019). It was first found in solar X-ray emission (Parks & Winckler 1969), then more and more QPP events are discovered in solar/stellar radiation intensity or flux over a broad range of wavelengths, i.e., radio emission (e.g., Ning et al. 2005; Kolotkov et al. 2015; Kupriyanova & Ratcliffe 2016; Nakariakov et al. 2018), Hα emission (e.g., Srivastava et al. 2008; Yang & Xiang 2016), Lyα emission (e.g., Milligan et al. 2017, 2019), extreme-ultraviolet (EUV) wave bands (e.g., Yuan et al. 2011, 2019; Li et al. 2018c; Hayes et al. 2019), and soft or hard X-ray (SXR or HXR) channels (e.g., Asai et al. 2001; Foullon et al. 2005; Ofman & Sui 2006; Li & Gan 2008; Ning 2014; Hayes et al. 2016). Moreover, the QPP has also been measured in spectroscopic observations, i.e., the regular and repeating variations in the Doppler velocity, line width, and intensity of spectral lines (e.g., Li & Zhang 2015; Wang et al. 2015; Tian et al. 2016; Brosius & Inglis 2018). Finally, the QPPs in solar flares are found to share some main frequencies with the quasi-periodic fast-propagating (QFP) magnetosonic waves (e.g., Liu et al. 2011; Shen & Liu 2012; Nisticò et al. 2014; Shen et al. 2018a), indicating their common origin (Yuan et al. 2013; Liu & Ofman 2014; Kumar et al. 2017; Shen et al. 2018b).

A typical QPP event can oscillate a few to tens of cycles, that is, the QPP can decay quickly (Wang et al. 2003; Anfinogentov et al. 2013) or could be persistent (decay-less; Tian et al. 2012, 2016). On the other hand, the oscillation period can be observed from milliseconds through seconds to dozens of minutes (Aschwanden et al. 1994; Schrijver et al. 2002; Tan et al. 2010; Inglis et al. 2016; Li & Zhang 2017; Kolotkov et al. 2018; Shen et al. 2018c). Sometimes, the QPP with a similar period has been detected in a wide range of wave bands (Dolla et al. 2012; Li et al. 2015), while the QPP with multi-periods has also been found in a same flare event (Inglis & Nakariakov 2009; Zimovets & Struminsky 2010; Chowdhury et al. 2015; Kolotkov et al. 2015). More specifically, the period ratio typically deviates from two, which might be attributed to the highly dispersive magnetohydrodynamic (MHD) mode, or the stratification of plasma density (e.g., Andries et al. 2005), or the expansion of flaring loop (e.g., Verth and Erdélyi 2008). The signature of QPP can be discovered in all phases of solar flares, such as precursor (Tan et al. 2016), impulsive phase (Li et al. 2017), and gradual phase (Li et al. 2018b). Moreover, different periods have been already found to be presented at different phases of the same flare event (Hayes et al. 2016; Dennis et al. 2017).

Statistical studies show that 80% of the X-class flares exhibit the signature of QPPs in the Geostationary Operational Environmental Satellite (GOES) X-ray channels during the impulsive phase (Simões et al. 2015). However, the generation mechanism of the QPP is still highly debated, which strongly depends on the observed period and wavelength (Aschwanden et al. 1994; Nakariakov & Melnikov 2009; Inglis & Dennis 2012; McLaughlin et al. 2018). Generally, the QPP detected in nonthermal emission such as microwave or HXR channel is thought to be related to the electron beam, which is accelerated by a periodic process of energy release during flare eruptions (Kliem et al. 2000; Asai et al. 2001; Inglis & Nakariakov 2009; Murray et al. 2009). On the other hand, the QPP with a short period observed in radio emission is often associated with the dynamic interaction between energetic

particles and waves, while a long-period QPP seen in the white light or EUV wave bands is supposed to be associated with the dynamic of emitting plasmas in solar active region or the whole Sun (Aschwanden 1987; Chen & Priest 2006; Nakariakov et al. 2006; Nakariakov & Melnikov 2009). Briefly, the QPP can be directly driven by an MHD wave in slow, kink, or sausage modes (Nakariakov et al. 2006, 2016; Reznikova & Shibasaki 2011; Van Doorsselaere et al. 2016), it could also be caused by a process of repetitive magnetic reconnection, which might be either spontaneous (such as magnetic dripping) or induced, i.e., by MHD oscillations (McLaughlin et al. 2009, 2018; Murray et al. 2009; Thurgood et al. 2017).

Lyα is a neutral hydrogen line at 1216 Å in the chromosphere, and it is the most prominent emission line in solar UV spectrum during flare eruptions (Woods et al. 2004; Allred et al. 2005; Milligan et al. 2012, 2014; Milligan & Chamberlin 2016). It is believed that the fluctuations in Lyα emission can cause the changes in planetary atmospheres during the high-activity period. Therefore, it is important to investigate the variability of Lyα emission during solar flares, which may be helpful for assessing its relative effect (see, Milligan et al. 2012, 2019; Milligan & Chamberlin 2016). However, what is not extensively studied is the temporal variation in Lyα emission during solar flares since it was first reported by Canfield & van Hoosier (1980), which is due to the limitation of the observational instruments. There are apparently very few studies of QPPs related to the Lyα emission. Milligan et al. (2017) first detected the QPP with a period of about 3 minutes in full-disk Lyα and Lyman continuum (LyC) emission during the impulsive phase of an X2.2 flare. Then they reported a 4.4 minute QPP in full-disk Lyα emission during the impulsive phase of an X1.1 flare. Both of these two QPPs are attributed to the acoustic waves induced by solar flares (Milligan et al. 2019).

The one minute QPP has been detected in full-disk SXR flux during a solar flare (e.g., Ning 2017; Hayes et al. 2019), and the QPP with periods of 3 and 4.4 minutes has been detected in the full-disk Lyα emission (Milligan et al. 2017, 2019) during two flares. In this paper, we discovered the 1 minute QPP in Lyα, EUV, and X-ray emission during two solar flares. Our finding could provide an observational constraint for the QPP generation mechanism. The observations in this paper are taken from the joint instruments, i.e., the EUV Sensor (EUVS; Viereck et al. 2007) and the X-Ray Sensor (XRS; Hanser & Sellers 1996) aboard the GOES, and the Atmospheric Imaging Assembly (AIA; Lemen et al. 2012) on board the Solar Dynamics Observatory (SDO).

2. Observations

Two solar flares are selected to investigate the QPP in this paper, both of which show a prominent QPP feature in the full-disk Lyα emission. One is an X1.7 flare on 2012 January 27, and takes place on the active region of NOAA 11402. The other is a C1.6 flare on 2016 February 8, occurring in the active region of NOAA 12492. Both of them are well recorded by the GOES/XRS, GOES/EUVS, and SDO/AIA, as seen in Table 1.

Figures 1 (a)–(d) show the EUV images in AIA 94 and 304 Å at around 17:45 UT and 18:45 UT on 2012 January 27, respectively. The flare occurs on the solar limb. The magenta box outlines the local region, which is used to integrate the flare flux in AIA 94 and 304 Å. Due to the saturation effect during the flare period, only short-exposure images with a temporal cadence of ~24 s are used here (Lemen et al. 2012; Ning 2017). Panel (e) presents the full-disk light curves in Lyα (black), SXR 1–8 Å (red), and 0.5–4 Å (blue) emission recorded by the GOES. The GOES 1–8 Å flux shows that an X1.7 flare starts to increase at roughly 18:05 UT, which could be identified as the onset time of this flare. On the other hand, a small but well-developed SXR peak appears at around 17:50 UT (red arrow), which is a bit earlier than the onset time of solar flare. The small pulse can also be found in GOES 0.5–4 Å and Lyα line flux, which is more prominent. However, these three GOES light curves are measured from the whole Sun. To determine if the small pulse is related to the X1.7 flare, we then plot the local EUV flux using the spatially resolved SDO/AIA observations. Similar to the full-disk GOES flux, the local light curves in AIA 94 Å (green) and 304 Å (orange) also show the small pulse before the flare onset time. In particular, the pulse in Lyα emission and AIA 304 Å is a little earlier but much more pronounced than that in GOES SXR channels and AIA 94 Å. Therefore, the small pulse occurring just before the flare onset could be considered as a flare precursor (Benz et al. 2017; Li et al. 2018a; Battaglia et al. 2019; Shen et al. 2019), which can be caused by an external reconnection as described in the magnetic breakout model (see Shen et al. 2012; Chen et al. 2016). Moreover, it is thought to play an important role in triggering the major flare (e.g., Priest & Forbes 2002; Lin et al. 2005; Zhou et al. 2019).

Figures 2 (a)–(d) present AIA EUV images in 94 and 304 Å at about 05:10 UT and 05:30 UT on 2016 February 8. The flare takes place near the solar disk center. Two magenta boxes (L and S) mark two bright regions used to integrate the local EUV fluxes. The flare consists of a circular flare ribbon and a bright inner flare ribbon, which is associated with negative magnetic polarities (blue contours) outside and positive magnetic polarities (yellow contours) inside, as shown in the solid box (L) in panel (d). Here the positive and negative magnetic fields were derived from the line-of-sight magnetogram, measured by the Helioseismic and Magnetic Imager (Schou et al. 2012). Thus, the C1.6 flare can be identified as a circular-ribbon flare (Ichimoto & Kurokawa 1984; Masson et al. 2009; Zhang et al. 2016). Panel (e) shows the full-disk GOES flux in Lyα (black) and SXR (red and blue) emission. Similar to the X1.7 flare, the GOES light curves also show a small and well-developed peak before the flare onset time, such as ~05:22 UT. Then we plot the local EUV light curves integrated over a large bright region (L) in AIA 94 Å (solid green) and 304 Å (orange). They both exhibit the flare peak after ~05:22 UT, but they lack the small peak before the flare onset time. On the other hand, the small peak can be found in a small bright region (S) in AIA 94 Å, as shown by a green dashed line. The observational fact suggests that the small pulse in SXR channels could be a solar

Table 1
The Metrics of Instruments Used in This Study

Instrument	Wavelength	Cadence (s)	Channel
GOES/EUVS	1216 Å	~11	Lyα
GOES/XRS	1–8 Å	~2	SXR
	0.5–4.0 Å	~2	SXR
SDO/AIA	94 Å	12	EUV
	304 Å	12	EUV

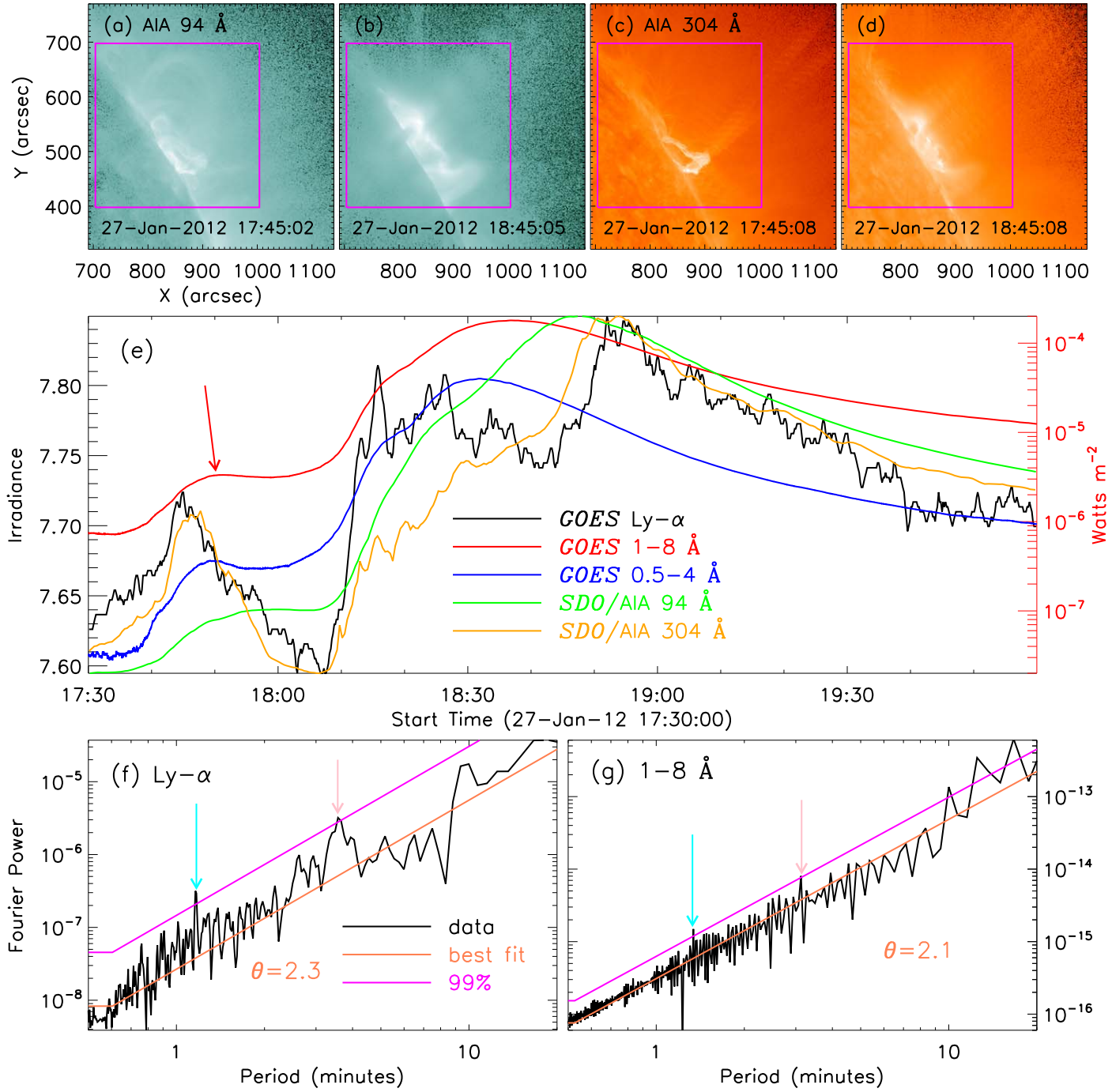

Figure 1. Overview of the solar flare on 2012 January 27. Panels (a)−(d): AIA images in 94 and 304 Å. The magenta box marks the flare region used to integrate the local EUV flux. Panel (e): Full-disk flux in Lyα (black), GOES 1–8 Å (red), and 0.5–4.0 Å (blue), the local flux in AIA 94 Å (green) and 304 Å (orange). Panels (f)−(g): Fourier power spectra derived from the Lyα and GOES 1–8 Å. The coral and magenta lines indicate the best-fit results and the confidence levels at 99%, respectively. The cyan and pink arrows indicate the periods above the confidence level.

microflare (Hannah et al. 2011; Nakariakov et al. 2018) rather than a flare precursor.

3. Data Reduction and Results

To examine the QPP feature in these two flares, the fast Fourier transform method (see, Ning 2017) is performed to the original light curves to obtain the Fourier spectrum in GOES Lyα and SXR channels, as shown in the panels (f) and (g) of Figures 1 and 2. In the astrophysical observations (Vaughan 2005; Pugh et al. 2017; Wang et al. 2020), the term "red noise" is often described by a power-law model in the Fourier power spectrum at longer periods, i.e., $P(T) \sim T^{\theta}$, where T is the period, θ represents a slope in the log–log coordinate system. While a white noise often refers to the flat spectrum at the shorter-period end. In the solar atmosphere, it is a very common observational phenomenon of such superposition of red and white noises, which are dominated at longer and shorter periods, respectively (e.g., Inglis et al. 2015; Kolotkov et al. 2016; Ning 2017; Li et al. 2020; Liang et al. 2020).

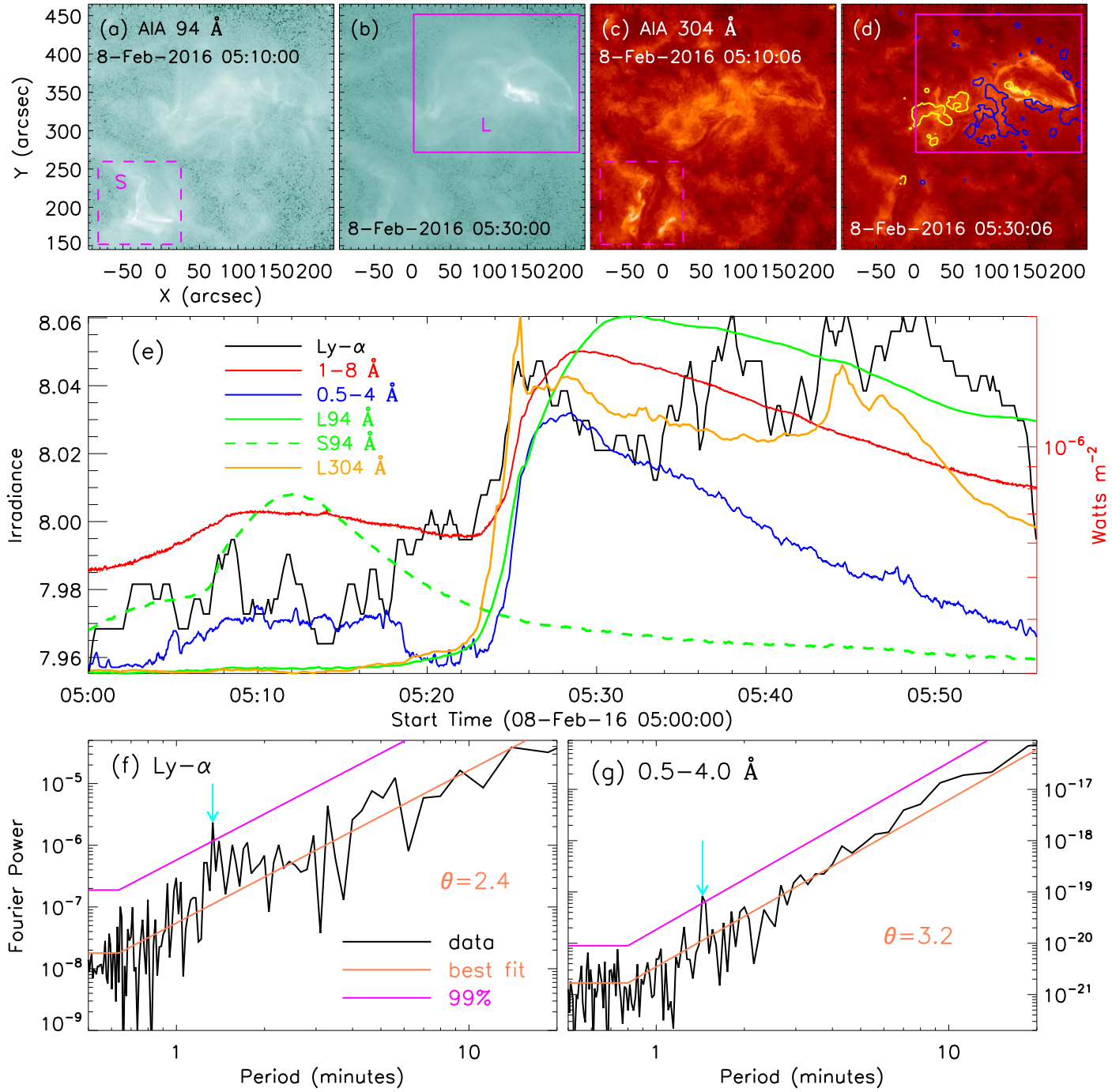

Figure 2. Overview of solar flares on 2016 February 8. Panels (a)–(d): AIA images in 94 and 304 Å. The yellow and blue contours represent the positive and negative magnetic fields at the levels of ±100 G. The magenta boxes mark the bright regions used to integrate the local EUV flux. Panel (e): Full-disk flux in Lyα (black), GOES 1–8 Å (red), and 0.5–4.0 Å (blue), the local flux in AIA 94 Å (green) and 304 Å (orange). Panels (f)–(g): Fourier power spectra derived from the Lyα and GOES 0.5–4 Å. The coral and magenta lines indicate the best-fit results and the confidence levels at 99%, respectively. The cyan arrow indicates the period above the confidence level.

Figures 1 (f) and (g) present Fourier power spectra of the X1.7 flare in Lyα and GOES 1–8 Å channels. The double peaks at roughly 1 and 3 minutes (cyan and pink arrows) are found to exceed the confidence level of 99% (magenta line) in these two power-law spectra, suggesting two periods in this flare-related QPP. We also notice much longer periods (>10 minutes) appearing in GOES 1–8 Å, which is out of the scope of this study, because it is absent in Lyα emission. Figure 2 (f) and (g) shows a similar Fourier power spectrum but for the C1.6 flare, and only one peak at around 1 minute can be detected to be above the 99% confidence level in the two power-law spectra, implying a 1 minute QPP in this C1.6 flare. The 3 minute QPP in Lyα emission has been reported by Milligan et al. (2017). Therefore, we focus on the QPP with a shorter period of ∼1 minute in this paper.

To investigate the 1 minute QPP of these two flares in detail, the wavelet analysis (e.g., Torrence & Compo 1998) is performed on the detrended light curve after removing a

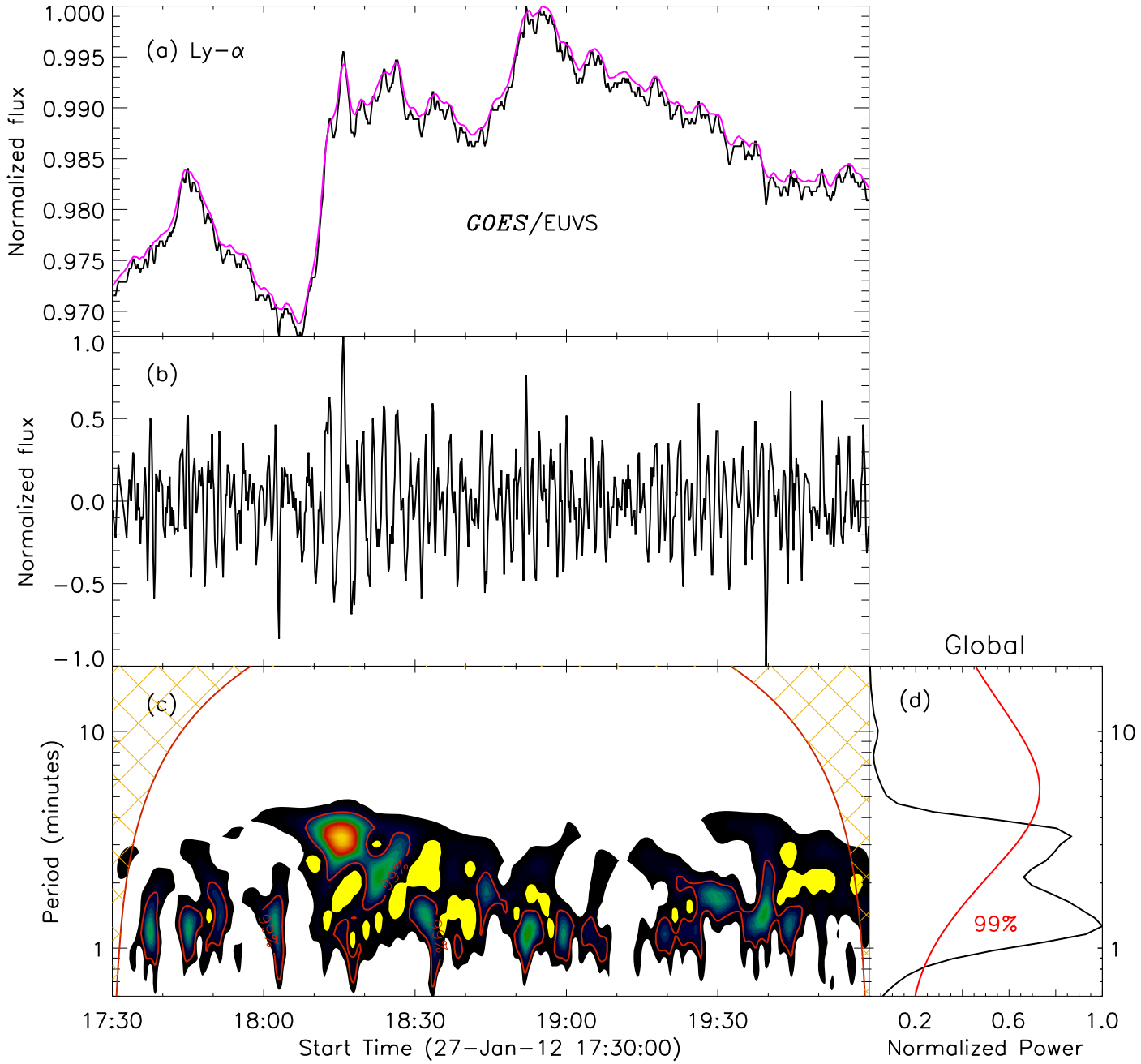

Figure 3. Wavelet analysis result in Lyα line of the X1.7 flare. Panel (a): Normalized original (black) and trended (magenta) light curves. Panel (b): Normalized detrended light curve. Panels (c) and (d): The wavelet power spectrum and the global wavelet power. The red lines indicate significance levels of 99%.

$\sim$110 s running average (see, i.e., Yuan et al. 2011; Tian et al. 2016). The detrended light curve is used here because we thereby enhance the short-period QPP to $\sim$1 minute and suppress the long-period trend; the discussion and justification of this method has been reported in detail by Gruber et al. (2011), Kupriyanova et al. (2010), Auchère et al. (2016), Dominique et al. (2018a), etc.

Figure 3 shows the wavelet analysis result of the X1.7 flare in the full-disk Lyα emission. Panel (a) displays the normalized light curve (black) in the Lyα emission from $\sim$17:30 UT to $\sim$20:00 UT on 2012 January 27, and its trended light curve is overplotted with a magenta line. Panel (b) gives the normalized detrended light curve, and it is characterized by a series of repeat and regular peaks, which could be regarded as the signature of QPP. Then, the oscillation period can be determined from the wavelet power spectrum and the global wavelet power, as shown in panels (c) and (d). They both exhibit double periods, i.e., a shorter period of $\sim$1 minute and a longer period of $\sim$3 minutes, which are consistent with the Fourier analysis result in Figure 1 (f). Moreover, the 1 minute QPP can be discovered between $\sim$17:35 UT and 19:40 UT, which is ranging from the flare precursor through the impulsive phase to the gradual phase. However, the 3 minute QPP only appears during the impulsive phase ($\sim$18:05 UT−18:30 UT), which is similar to previous findings (e.g., Milligan et al. 2017, 2019).

Figure 4 presents the wavelet analysis result in the full-disk SXR 1–8 Å flux of the X1.7 flare. The left panels show the

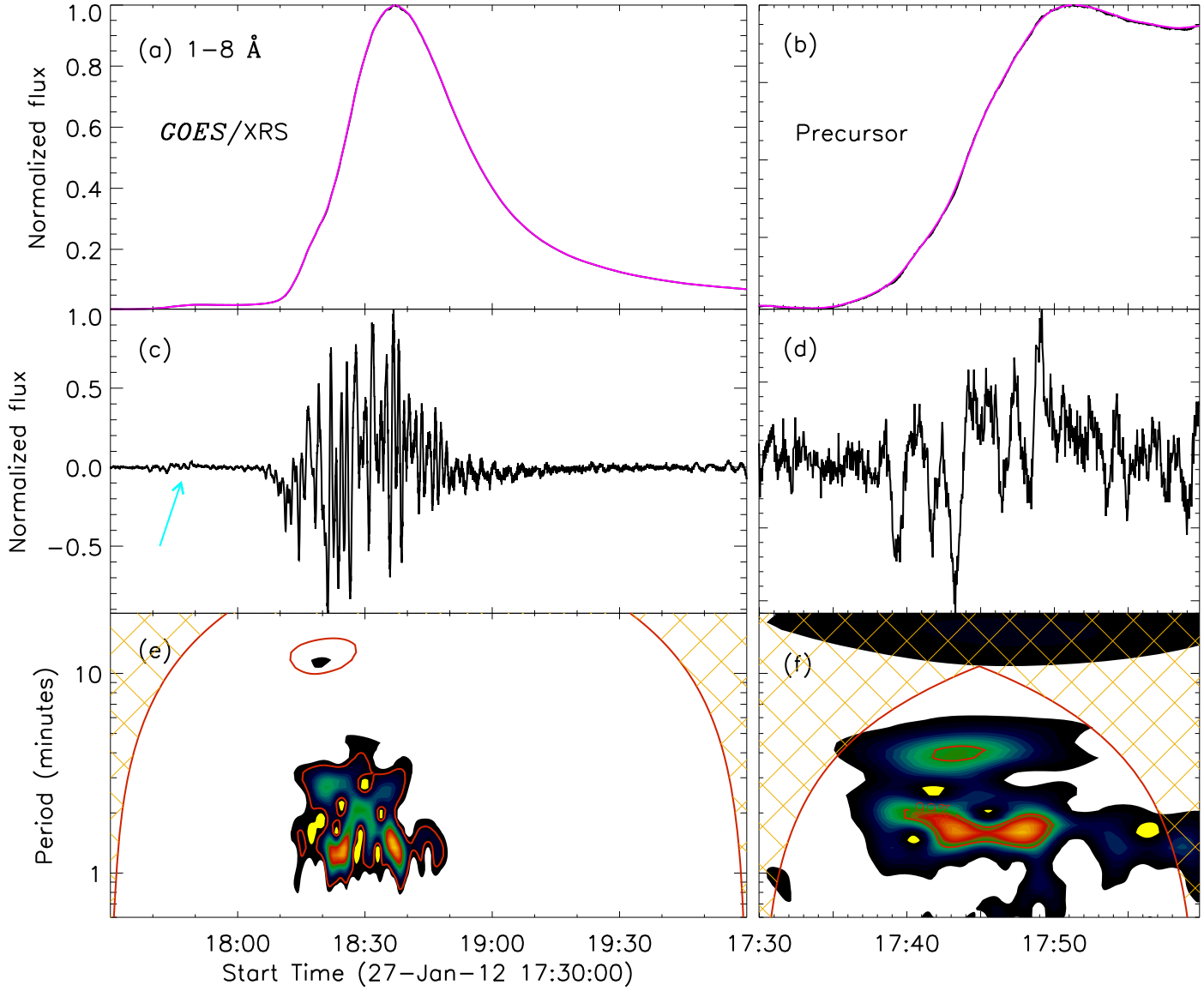

Figure 4. Wavelet analysis result in GOES 1–8 Å of the X1.7 flare. Panels (a) and (b): Normalized original (black) and trended (magenta) light curves. Panels (c) and (d): Normalized detrended light curve. Panels (e) and (f): The wavelet power spectra. The red lines indicate significance levels of 99%.

normalized light curve (a), the normalized detrended light curve (c) and the wavelet power spectrum (e) from ∼17:30 UT to ∼20:00 UT. It can be seen that both the 1 and 3 minute QPPs tend to appear between ∼18:10 UT and ∼18:50 UT. There is not any apparent signature of QPP before 18:00 UT, which could be attributed to the fact that the SXR radiation during the solar flare is much stronger than that during the flare precursor, as shown in panel (a). A series of repeat but very small peaks can be found between ∼17:35 UT and ∼17:50 UT, as indicated with a cyan arrow in panel (c). Therefore, the SXR flux during the flare precursor is selected to perform the wavelet analysis, as shown in the right panels. The original and detrended light curves are given in panels (b) and (d), and the QPP feature is pronounced in the detrended light curve. The 1 minute QPP can be found between ∼17:35 UT and ∼17:50 UT in the wavelet power spectrum, as shown in panel (f).

Figure 5 shows the similar wavelet analysis result of the C1.6 flare in the full-disk Lyα emission. The normalized original (black) and trended (magenta) light curves from 05:00 UT to 05:56 UT are given in panel (a). Panel (b) presents the normalized detrended light curve, which exhibits a pronounced QPP feature. The 1 minute period can appear simultaneously in the wavelet power spectrum (c) and the global wavelet power (d), and it could remain from the impulsive to gradual phases, i.e., from ∼05:15 UT to ∼05:45 UT. We also notice that the 1 minute period can be found between around 05:05 UT and 05:10 UT, which is believed as a microflare. However, the wavelet power, as well as the Ly-a emission, is relatively weak. Thus, it is not considered in this work. The similar wavelet analysis result can be derived from the full-disk SXR flux measured by GOES/XRS, as shown in Figure 6. It exhibits a strong QPP with a period of roughly 1 minute during the impulsive phase, i.e., between ∼05:20 UT and 05:30 UT. It also displays a weak signature of 1 minute QPP during the gradual phase. We also notice that the onset time of QPP in SXR channel is later than that seen in Lyα emission, which is attributed to the time delay between the SXR flux and the Lyα irradiance (see also Milligan & Chamberlin 2016; Chamberlin et al. 2018).

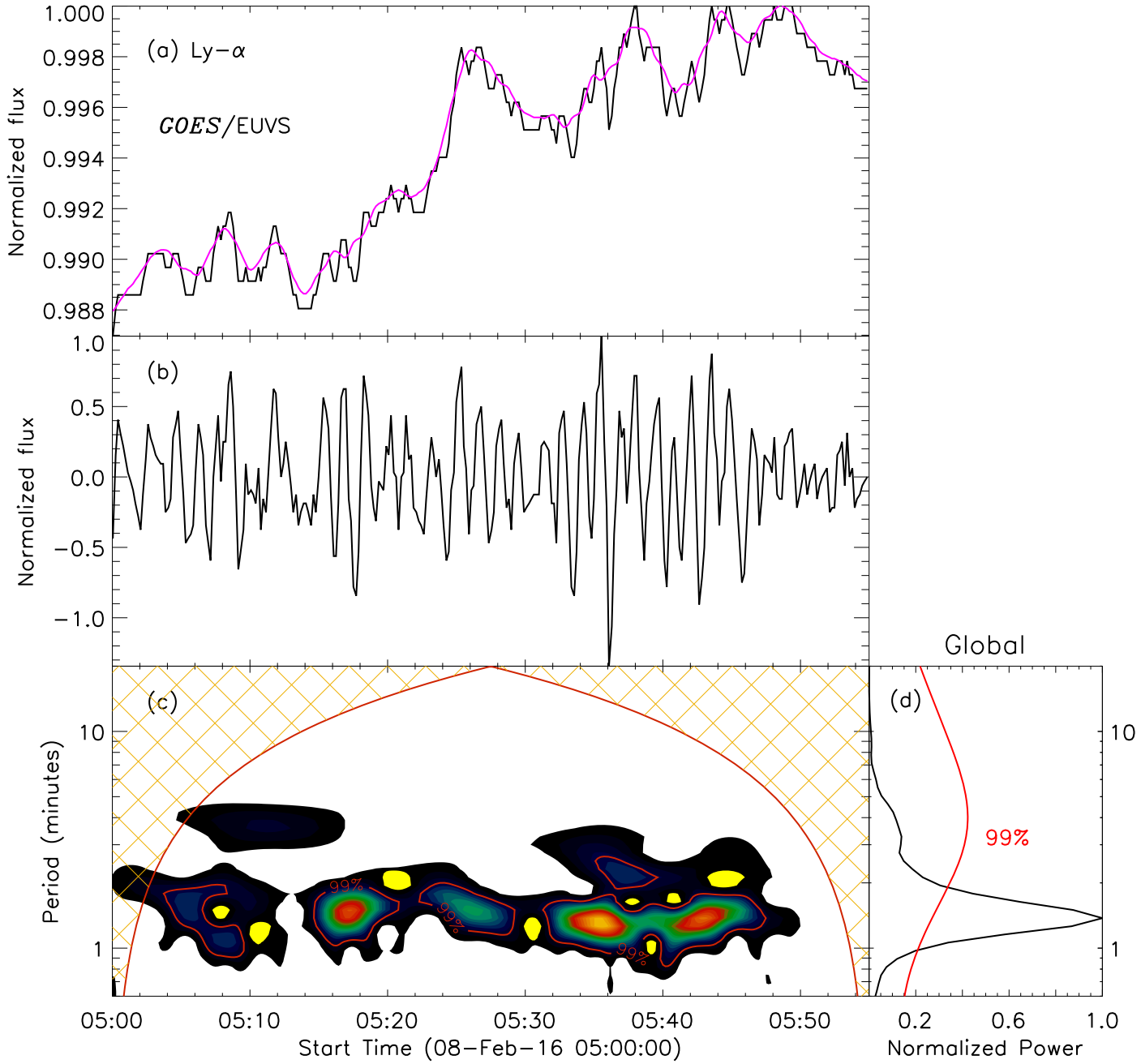

Figure 5. Wavelet analysis result in Lyα line of the C1.6 flare. Panel (a): Normalized original (black) and trended (magenta) light curves. Panel (b): Normalized detrended light curve. Panels (c) and (d): The wavelet power spectrum and the global wavelet power. The red lines indicate significance levels of 99%.

The 1 minute QPP is discovered in the full-disk light curves in the Lyα and SXR channels. Thanks to the high-spatial resolution imaging observations from SDO/AIA, we can obtain the local EUV flux such as 304 Å. Figure 7 shows the Fourier spectra in local AIA 304 Å of the X1.7 (a) and C1.6 (b) flares, respectively. Both of these two flares display a pronounced QPP feature at a period of roughly 1 minute, but only the X1.7 flare appear in the 3 minute QPP. All these observational results based on the local EUV flux agree well with previous findings derived from the full-disk light curves recorded by the GOES. Finally, the ARIMA model and the SARIMA model with a periodic component (e.g., Box et al. 2015; Hyndman & Athanasopoulos 2018) are applied to the light curve of the solar flare, respectively. The Akaike information criterion of the latter was better than the former model, suggesting that the true periodicity is present in this work.

4. Conclusion and Discussion

Using the GOES/EUVS observations, we discovered the 1 minute QPP in the Lyα emission during two solar flares, i.e., an X1.7 flare, and a C1.6 circular-ribbon flare. Moreover, the 1 minute QPP can be detected during the whole flare phases, such as flare precursor, impulsive, and gradual phases. On the other hand, we could not detect the similar 1 minute QPP in Lyα light curves before and after the two flares under study, which indicates that the 1 minute QPP mainly comes from the flare radiation rather than the background emission of the Sun.

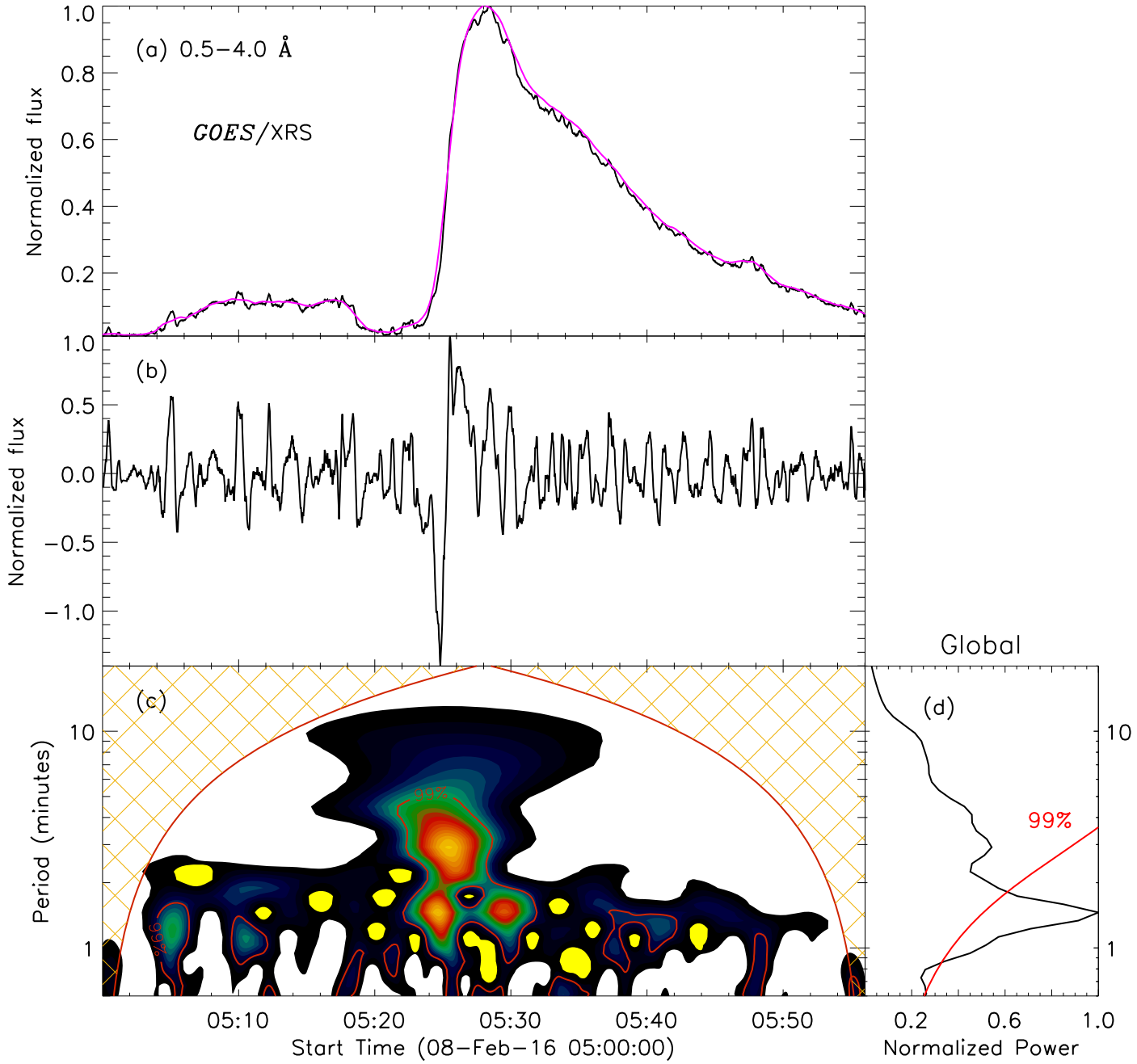

Figure 6. Wavelet analysis result in GOES 0.5–4 Å of the C1.6 flare. Panel (a): Normalized original (black) and trended (magenta) light curves. Panel (b): Normalized detrended light curve. Panels (c) and (d): The wavelet power spectrum and the global wavelet power. The red lines indicate significance levels of 99%.

It is well known that the neutral hydrogen Lyα is the strongest emission line in the solar UV spectrum, which shows a significant enhancement during solar flares (e.g., Woods et al. 2004; Milligan et al. 2012, 2019). However, the Lyα variability of solar flares has not yet been investigated extensively, mainly due to the limited observational instruments (Kretzschmar et al. 2013; Milligan et al. 2019). Therefore, the QPP in Lyα emission is rarely studied. Milligan et al. (2017) first found the 3 minute QPP in full-disk Lyα and LyC emission during the impulsive phase of an X2.2 flare, which was attributed to be the acoustic waves in the chromosphere. Later on, they discovered another 4.4 minute QPP in Lyα emission from the full-disk irradiance during the impulsive phase of an X1.1 flare at solar limb (Milligan et al. 2019). In our studies, a similar 3 minute QPP is observed during the impulsive phase of the X1.7 flare. However, it failed to be detected in the C1.6 flare, which might be due to its weak radiation and short lifetime.

The QPP with a period of around 1 minute can also be found in X-ray and EUV wave bands, such as GOES 1–8 Å, 0.5–4 Å, and AIA 304 Å. The 1 minute QPP has been extensively studied during an X1.6 flare on 2014 September 10 in multiple wavelengths, such as SXR, HXR, and EUV wave bands, and it can be found during the impulsive and gradual phases (Ning 2017). On the other hand, the 1 minute QPP was found in SXR flux during the impulsive phase of an X8.2 flare on 2017 September 10 (Hayes et al. 2019). Besides that, we further detected the 1 minute QPP in Lyα emission during the precursor of an X-class flare. The QPP with a period

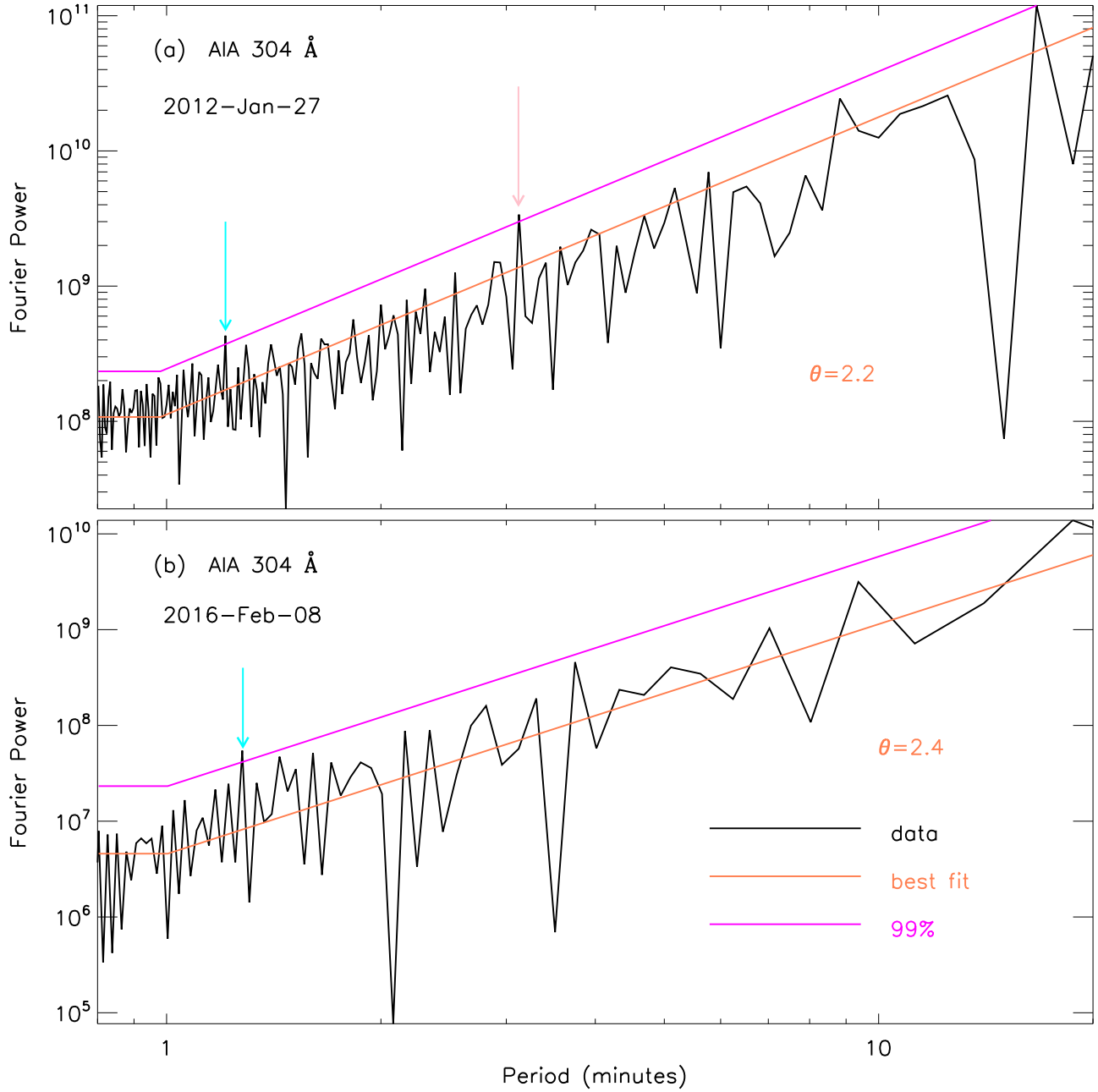

Figure 7. Fourier spectra in AIA 304 Å for the flares on 2016 January 27 (a) and 2016 February 8 (b), respectively. The coral and magenta lines indicate the best-fit results and the confidence levels of 99%.

of 32–42 s has been reported during a C3.1 circular-ribbon flare in the Si IV line intensity and SXR derivative flux (Zhang et al. 2016). In this paper, we found the 1 minute QPP in the Lyα line and SXR/EUV flux during a C-class circular-ribbon flare.

It is worthwhile to stress that the 1 minute QPP can be clearly observed in the Lyα emission from the precursor through impulsive to gradual phases of the X1.7 flare, as shown in Figure 3. However, the QPP detected in the SXR flux during the impulsive phase shows a much stronger signature when comparing to that detected during the flare precursor phase, as seen in Figure 4. This could be associated with enhancements of the flare radiation in different wavelengths. It can be seen that the full-disk SXR irradiance during the flare impulsive phase is much stronger than that during the flare precursor, i.e., nearly 100 times, as indicated by the red line in the panel (e) of Figure 1. On the other hand, the Lyα enhancement during the solar flare is fairly weak. A statistical study of 477 M- and X-class flares suggests that 95% of these large flares show a $\leqslant$10% increase in the Lyα emission above their background, with a maximum enhancement of $\sim$30% (e.g., Milligan et al. 2019). The similar Lyα contrast during solar flares is also discovered by Brekke et al. (1996) and Woods et al. (2004). Moreover, a much smaller increase such as $<$1% in Lyα emission during solar flares is detected by the Large Yield Radiometer (see, i.e., Kretzschmar et al. 2013; Raulin et al. 2013). All these findings are consistent with our observations, i.e., less than 10% enhancement compared to its background, as indicated with the black line in Figure 1 (e).

We address here the possible generation mechanism of the 1 minute QPP in Lyα emission. It could not depend on the nonthermal electron produced by a periodic magnetic reconnection (Nakariakov & Melnikov 2009; Milligan et al. 2017) due to the fact that it could be detected from the flare precursor through impulsive to gradual phase (e.g., Tian et al. 2016). Conversely, given the fact that the 1 minute QPP can be discovered during the whole phases of solar flares, it is most likely to be driven by a self-oscillation process of the spontaneous magnetic reconnection, i.e., magnetic dripping (e.g., Nakariakov et al. 2010; McLaughlin et al. 2018). On the other hand, it might also be interpreted as the MHD wave (Reznikova & Shibasaki 2011; Nakariakov et al. 2016; Van Doorsselaere et al. 2016). The 1 minute QPP in full-disk SXR/HXR flux and local EUV emission has been found to originate from the flare footpoints (Ning 2017), where the Lyα emission was supposed to be generated (Allred et al. 2005; Rubio da Costa et al. 2009; Chamberlin et al. 2018; Dominique et al. 2018b). Therefore, the MHD oscillation at footpoints could also be used to explain the 1 minute QPP, i.e., the sausage wave (e.g., Tian et al. 2016; Kolotkov et al. 2018) or the acoustic wave (e.g., Milligan et al. 2017, 2019). However, it is impossible to determine the mode of MHD wave, since the imaging observations in Lyα emission are very few. So, the oscillation location and physical parameters such as the plasma density is still hard to be determined. The future instruments such as the Extreme Ultraviolet Imager (Schühle et al. 2011) on board the Solar Orbiter (Marsch et al. 2005) and the Lyα Solar Telescope (Feng et al. 2019; Li et al. 2019) on board the Advanced Space-based Solar Observatory (Gan et al. 2019; Huang et al. 2019), are promising to solve this issue.

Finally, we want to stress that the shorter period of the flare-related QPP ranges between $\sim$1.1 and 1.4 minutes, while the longer period varies from $\sim$3.2 to $\sim$3.5 minutes, as indicated by the peaks of the Fourier power spectra in Figures 1, 2, and 7. However, there are diffuse period ranges in wavelet power spectra, as shown in Figures 3–5. For simplicity, we regarded them as 1 or 3 minute periods in this paper, which were similar to previous findings (e.g., Milligan et al. 2017; Ning 2017). Using the SDO/AIA observations, the QFP magnetosonic wave trains after a C2.0 flare were found to have a common period of $\sim$80 $\pm$ 10 s (see Shen et al. 2013), which is similar to the 1 minute QPP we found here.. Moreover, the quasi-periods both in their QFPs and our flare-related QPPs were attributed to some periodic processes in magnetic reconnection (see also Liu et al. 2011; Yuan et al. 2013; Kumar et al. 2017). As a next-step work, we will search for QFP wave trains with a period of $\sim$1 minute in the future.

We thank the anonymous referee for valuable comments. The authors would like to acknowledge Profs. V. Nakariakov, S. Feng, H. Tian, Y. Ding, and J. Chae, for their inspiring discussions. We thank the teams of GOES/EUVS, GOES/XRS, and SDO/AIA for their open data use policy. This work is supported by NSFC under grants 11973092, 11921003, 11973012, 11873095, 11790302, 11790300, 11729301, 11773061, and U1731241, U1931138, the Youth Fund of Jiangsu No. BK20171108, and KLSA202003, as well as CAS Strategic Pioneer Program on Space Science, grant No. XDA15052200, XDA15320103, and XDA15320301. D.L. is also supported by the Specialized Research Fund for State Key Laboratories. This work is also supported by the mobility grant of Sino-German Science Center M-0068, and National key research and development program 2018YFA0404202, and the Laboratory No. 2010DP173032.

ORCID iDs

Dong Li https://orcid.org/0000-0002-4538-9350
Lei Lu https://orcid.org/0000-0002-3032-6066
Zongjun Ning https://orcid.org/0000-0002-9893-4711

References

Allred, J. C., Hawley, S. L., Abbett, W. P., et al. 2005, ApJ, 630, 573
Andries, J., Goossens, M., Hollweg, J. V., et al. 2005, A&A, 430, 1109
Anfinogentov, S., Nakariakov, V. M., Mathioudakis, M., et al. 2013, ApJ, 773, 156
Asai, A., Shimojo, M., Isobe, H., et al. 2001, ApJL, 562, L103
Aschwanden, M. J. 1987, SoPh, 111, 113
Aschwanden, M. J., Benz, A. O., Dennis, B. R., et al. 1994, ApJS, 90, 631
Auchère, F., Froment, C., Bocchialini, K., et al. 2016, ApJ, 825, 110
Battaglia, M., Kontar, E. P., & Motorina, G. 2019, ApJ, 872, 204
Benz, A. O., Battaglia, M., & Güdel, M. 2017, SoPh, 292, 151
Box, G. E. P., Jenkins, G. M., Reinsel, G. C., & Ljung, G. M. 2015, Time Series Analysis: Forecasting and Control (5th ed.; Hoboken, New Jersey: John Wiley Sons)
Brekke, P., Rottman, G. J., Fontenla, J., et al. 1996, ApJ, 468, 418
Brosius, J. W., & Inglis, A. R. 2018, ApJ, 867, 85
Canfield, R. C., & van Hoosier, M. E. 1980, SoPh, 67, 339
Chamberlin, P. C., Woods, T. N., Didkovsky, L., et al. 2018, SpWea, 16, 1470
Chen, P. F., & Priest, E. R. 2006, SoPh, 238, 313
Chen, Y., Du, G., Zhao, D., et al. 2016, ApJL, 820, L37
Chowdhury, P., Srivastava, A. K., Dwivedi, B. N., et al. 2015, AdSpR, 56, 2769
Dennis, B. R., Tolbert, A. K., Inglis, A., et al. 2017, ApJ, 836, 84
Dolla, L., Marqué, C., Seaton, D. B., et al. 2012, ApJL, 749, L16
Dominique, M., Zhukov, A. N., Dolla, L., et al. 2018a, SoPh, 293, 61
Dominique, M., Zhukov, A. N., Heinzel, P., et al. 2018b, ApJL, 867, L24
Feng, L., Li, H., Chen, B., et al. 2019, RAA, 19, 162
Foullon, C., Verwichte, E., Nakariakov, V. M., et al. 2005, A&A, 440, L59
Gan, W.-Q., Zhu, C., Deng, Y.-Y., et al. 2019, RAA, 19, 156
Gruber, D., Lachowicz, P., Bissaldi, E., et al. 2011, A&A, 533, A61
Hannah, I. G., Hudson, H. S., Battaglia, M., et al. 2011, SSRv, 159, 263
Hanser, F. A., & Morel, P. R. 1996, NASA Technical Report, 21804
Hayes, L. A., Gallagher, P. T., Dennis, B. R., et al. 2016, ApJL, 827, L30
Hayes, L. A., Gallagher, P. T., Dennis, B. R., et al. 2019, ApJ, 875, 33
Huang, Y., Li, H., Gan, W.-Q., et al. 2019, RAA, 19, 164
Hyndman, R. J., & Athanasopoulos, G. 2018, Forecasting: Principles and Practice (2nd ed.; Melbourne: OTexts) Australia.OTexts.com/fpp2
Ichimoto, K., & Kurokawa, H. 1984, SoPh, 93, 105
Inglis, A. R., & Dennis, B. R. 2012, ApJ, 748, 139
Inglis, A. R., Ireland, J., Dennis, B. R., et al. 2016, ApJ, 833, 284
Inglis, A. R., Ireland, J., & Dominique, M. 2015, ApJ, 798, 108
Inglis, A. R., & Nakariakov, V. M. 2009, A&A, 493, 259
Kliem, B., Karlický, M., & Benz, A. O. 2000, A&A, 360, 715
Kolotkov, D. Y., Anfinogentov, S. A., & Nakariakov, V. M. 2016, A&A, 592, A153
Kolotkov, D. Y., Nakariakov, V. M., Kupriyanova, E. G., et al. 2015, A&A, 574, A53
Kolotkov, D. Y., Pugh, C. E., Broomhall, A.-M., et al. 2018, ApJL, 858, L3
Kretzschmar, M., Dominique, M., & Dammasch, I. E. 2013, SoPh, 286, 221
Kumar, P., Nakariakov, V. M., & Cho, K.-S. 2017, ApJ, 844, 149
Kupriyanova, E. G., Melnikov, V. F., Nakariakov, V. M., et al. 2010, SoPh, 267, 329
Kupriyanova, E. G., & Ratcliffe, H. 2016, AdSpR, 57, 1456
Lemen, J. R., Title, A. M., Akin, D. J., et al. 2012, SoPh, 275, 17
Li, D., Kolotkov, D. Y., Nakariakov, V. M., et al. 2020, ApJ, 888, 53
Li, D., Li, Y., Su, W., et al. 2018a, ApJ, 854, 26
Li, D., Ning, Z. J., & Zhang, Q. M. 2015, ApJ, 807, 72
Li, D., Yuan, D., Su, Y. N., et al. 2018b, A&A, 617, A86
Li, D., & Zhang, Q. M. 2017, MNRAS, 471, L6
Li, D., Zhang, Q. M., Huang, Y., et al. 2017, A&A, 597, L4
Li, H., Chen, B., Feng, L., et al. 2019, RAA, 19, 158
Li, L., Zhang, J., Peter, H., et al. 2018c, ApJL, 868, L33
Li, T., & Zhang, J. 2015, ApJL, 804, L8
Li, Y. P., & Gan, W. Q. 2008, SoPh, 247, 77

Liang, B., Meng, Y., Feng, S., et al. 2020, Ap&SS, 365, 40
Lin, J., Ko, Y.-K., Sui, L., et al. 2005, ApJ, 622, 1251
Liu, W., & Ofman, L. 2014, SoPh, 289, 3233
Liu, W., Title, A. M., Zhao, J., et al. 2011, ApJL, 736, L13
Marsch, E., Marsden, R., Harrison, R., et al. 2005, AdSpR, 36, 1360
Masson, S., Pariat, E., Aulanier, G., et al. 2009, ApJ, 700, 559
McLaughlin, J. A., De Moortel, I., Hood, A. W., et al. 2009, A&A, 493, 227
McLaughlin, J. A., Nakariakov, V. M., Dominique, M., et al. 2018, SSRv, 214, 45
Milligan, R. O., & Chamberlin, P. C. 2016, A&A, 587, A123
Milligan, R. O., Chamberlin, P. C., Hudson, H. S., et al. 2012, ApJL, 748, L14
Milligan, R. O., Fleck, B., Ireland, J., et al. 2017, ApJL, 848, L8
Milligan, R. O., Hudson, H. S., Chamberlin, P. C., et al. 2019, arXiv:1910.01364
Milligan, R. O., Kerr, G. S., Dennis, B. R., et al. 2014, ApJ, 793, 70
Murray, M. J., van Driel-Gesztelyi, L., & Baker, D. 2009, A&A, 494, 329
Nakariakov, V. M., Anfinogentov, S., Storozhenko, A. A., et al. 2018, ApJ, 859, 154
Nakariakov, V. M., Foullon, C., Verwichte, E., et al. 2006, A&A, 452, 343
Nakariakov, V. M., Inglis, A. R., Zimovets, I. V., et al. 2010, PPCF, 52, 124009
Nakariakov, V. M., & Melnikov, V. F. 2009, SSRv, 149, 119
Nakariakov, V. M., Pilipenko, V., Heilig, B., et al. 2016, SSRv, 200, 75
Ning, Z. 2014, SoPh, 289, 1239
Ning, Z. 2017, SoPh, 292, 11
Ning, Z., Ding, M. D., Wu, H. A., et al. 2005, A&A, 437, 691
Nisticò, G., Pascoe, D. J., & Nakariakov, V. M. 2014, A&A, 569, A12
Ofman, L., & Sui, L. 2006, ApJL, 644, L149
Parks, G. K., & Winckler, J. R. 1969, ApJL, 155, L117
Priest, E. R., & Forbes, T. G. 2002, A&ARv, 10, 313
Pugh, C. E., Broomhall, A.-M., & Nakariakov, V. M. 2017, A&A, 602, A47
Pugh, C. E., Broomhall, A.-M., & Nakariakov, V. M. 2019, A&A, 624, A65
Raulin, J.-P., Trottet, G., Kretzschmar, M., et al. 2013, JGRA, 118, 570
Reznikova, V. E., & Shibasaki, K. 2011, A&A, 525, A112
Rubio da Costa, F., Fletcher, L., Labrosse, N., et al. 2009, A&A, 507, 1005
Schou, J., Scherrer, P. H., Bush, R. I., et al. 2012, SoPh, 275, 229
Schrijver, C. J., Aschwanden, M. J., & Title, A. M. 2002, SoPh, 206, 69
Schühle, U., Halain, J.-P., Meining, S., et al. 2011, Proc. SPIE, 8148, 81480K
Shen, Y., & Liu, Y. 2012, ApJ, 753, 53
Shen, Y., Liu, Y., Song, T., et al. 2018a, ApJ, 853, 1
Shen, Y., Liu, Y., & Su, J. 2012, ApJ, 750, 12
Shen, Y., Qu, Z., Zhou, C., et al. 2019, ApJL, 885, L11
Shen, Y., Song, T., & Liu, Y. 2018b, MNRAS, 477, L6
Shen, Y., Tang, Z., Miao, Y., et al. 2018c, ApJL, 860, L8
Shen, Y.-D., Liu, Y., Su, J.-T., et al. 2013, SoPh, 288, 585
Simões, P. J. A., Hudson, H. S., & Fletcher, L. 2015, SoPh, 290, 3625
Srivastava, A. K., Zaqarashvili, T. V., Uddin, W., et al. 2008, MNRAS, 388, 1899
Tan, B., Yu, Z., Huang, J., et al. 2016, ApJ, 833, 206
Tan, B., Zhang, Y., Tan, C., et al. 2010, ApJ, 723, 25
Thurgood, J. O., Pontin, D. I., & McLaughlin, J. A. 2017, ApJ, 844, 2
Tian, H., McIntosh, S. W., Wang, T., et al. 2012, ApJ, 759, 144
Tian, H., Young, P. R., Reeves, K. K., et al. 2016, ApJL, 823, L16
Torrence, C., & Compo, G. P. 1998, BAMS, 79, 61
Van Doorsselaere, T., Kupriyanova, E. G., & Yuan, D. 2016, SoPh, 291, 3143
Vaughan, S. 2005, A&A, 431, 391
Verth, G., & Erdélyi, R. 2008, A&A, 486, 1015
Viereck, R., Hanser, F., Wise, J., et al. 2007, Proc. SPIE, 6689, 66890K
Wang, T., Ofman, L., Sun, X., et al. 2015, ApJL, 811, L13
Wang, T. J., Solanki, S. K., Curdt, W., et al. 2003, A&A, 406, 1105
Wang, Z.-K., Feng, S., Deng, L.-H., et al. 2020, RAA, 20, 006
Woods, T. N., Eparvier, F. G., Fontenla, J., et al. 2004, GeoRL, 31, L10802
Yang, S., & Xiang, Y. 2016, ApJL, 819, L24
Yuan, D., Feng, S., Li, D., et al. 2019, ApJL, 886, L25
Yuan, D., Nakariakov, V. M., Chorley, N., et al. 2011, A&A, 533, A116
Yuan, D., Shen, Y., Liu, Y., et al. 2013, A&A, 554, A144
Zhang, Q. M., Li, D., & Ning, Z. J. 2016, ApJ, 832, 65
Zhou, G. P., Tan, C. M., Su, Y. N., et al. 2019, ApJ, 873, 23
Zimovets, I. V., & Struminsky, A. B. 2010, SoPh, 263, 163